Desalination 526 (2022) 115516

Contents lists available at ScienceDirect

Desalination

journal homepage: www.elsevier.com/locate/desal

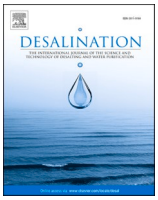

Performance evaluation and optimization of humidification–dehumidification desalination system for low-grade waste heat energy applications

Ravichandran Santosh [a,b], Chan Ho Yoo [c], Young-Deuk Kim [d,e,*]

[a] Energy & Environmental Engineering Laboratory, Department of Mechanical Engineering, Hanyang University, 55 Hanyangdaehak-ro, Sangnok-gu, Ansan, Gyeonggi-do 15588, Republic of Korea
[b] ERICA Industry-University Cooperation Foundation, Hanyang University, 55 Hanyangdaehak-ro, Sangnok-gu, Ansan, Gyeonggi-do 15588, Republic of Korea
[c] Department of Mechanical Design Engineering, Hanyang University, 222 Wangsimni-ro, Seongdong-gu, Seoul 04763, Republic of Korea
[d] Department of Mechanical Engineering, Hanyang University, 55 Hanyangdaehak-ro, Sangnok-gu, Ansan, Gyeonggi-do 15588, Republic of Korea
[e] BK21 FOUR ERICA-ACE Center, Hanyang University, 55 Hanyangdaehak-ro, Sangnok-gu, Ansan, Gyeonggi-do 15588, Republic of Korea

HIGHLIGHTS

- Low-grade waste heat is utilized to convert seawater into freshwater through HDH.
- The system is optimized for process conditions in conjunction with different packed humidifiers.
- Seawater is directly used as a coolant (25 °C) without precooling.
- The humidifier's surface area had a direct influence on freshwater productivity.
- The generated freshwater satisfies WHO and EPA drinking water standards.

ARTICLE INFO

Keywords:
Humidification–dehumidification
Waste heat
Desalination
Seawater
Potable water

ABSTRACT

A humidification–dehumidification desalination system powered by low-grade waste heat energy (45 °C–70 °C) was experimentally investigated. The seawater directly utilized as coolant (25 °C) for the dehumidifier was preheated by latent heat recovery from the water vapor produced by the humidifier. The effect of key performance-contributing factors such as the mass flow rate and temperature of the air and feed at the inlets of the humidifier and dehumidifier were evaluated and optimized. For a constant volume, the effect of the humidifier's surface area was evaluated comparatively considering different novel packing materials such as tri-pack rings, pall rings (diameter = 16 mm and 25 mm), saddle rings, and snowflake rings. It was determined that compared to other factors, air-related and water-related parameters influenced the humidifier and dehumidifier performance respectively. Maximum freshwater productivity of 1398 mL/h was achieved with 16 mm pall ring humidifier, owing to its improved wet area (188,000 m^2/m^3) under optimal conditions of air flow rate, feed flow rate, humidifier air inlet temperature, humidifier, and dehumidifier water inlet temperatures of 3.5 kg/min, 0.9 L/min, 70 °C, 55 °C, and 25 °C, respectively, with a dual-fluid preheating mechanism. Detailed chemical analysis revealed that the generated freshwater is potable.

1. Introduction

Water is a basic need for living beings to survive. However, freshwater resources are depleting rapidly owing to massive urbanization, climate change, and population growth [1]. In 2017, approximately 2.1 billion individuals worldwide did not have access to freshwater. This number is estimated to increase to approximately 7 billion by 2050 [2]. This scenario has resulted in an urgent need to identify alternate sources for satisfying the global water-related demands. Desalination is regarded as one of the most cost-effective technologies for satisfying freshwater

* Corresponding author at: Department of Mechanical Engineering, Hanyang University, 55 Hanyangdaehak-ro, Sangnok-gu, Ansan, Gyeonggi-do 15588, Republic of Korea.
E-mail address: youngdeuk@hanyang.ac.kr (Y.-D. Kim).

https://doi.org/10.1016/j.desal.2021.115516
Received 30 September 2021; Received in revised form 12 November 2021; Accepted 18 December 2021
Available online 3 January 2022

requirements worldwide [3]. In general, desalination can be categorized into membrane-based (reverse osmosis (RO), electrodialysis, forward osmosis, and ion exchange process) and thermal energy-based (multi-effect desalination, multi-stage flashing (MSF), vapor compression, and humidification–dehumidification (HDH)) technologies. Among these, RO and MSF are predominantly adopted for centralized freshwater production [4,5]. However, both these are highly energy-intensive (electricity or thermal) because these require specialized pressure and temperature conditions in conjunction with complex systems [6]. Most of the established RO and MSF desalination plants are fossil fuel-powered, which further increases the pressure on the requirement and utilization of fossil fuel for desalination [5]. It is noteworthy that 10,000 tons of oil are utilized annually for freshwater production of 1000 m^3/day [7]. In addition, brine production and disposal is a significant impediment that the aforementioned technologies have to address. Therefore, intensive efforts have been undertaken in the field of HDH desalination technology over the past decade to develop cost-effective and sustainable solutions [8,9]. Of all the desalination techniques, HDH has been established to be suitable for decentralized freshwater production owing to its advantages such as low operating pressure (~1.013 bar) and temperature (~80 °C), construction using local inexpensive materials, and convenient operation and maintenance [10,11]. Considering the elevated global electrical energy demand and economy, significant research works have been undertaken recently on the integration of HDH desalination systems with solar and waste heat energy to make the entire process economically viable and environmentally friendly [12,13].

Solar energy-powered HDH desalination systems are equipped with specialized solar collectors for preheating the water or/and air that plays a significant role in the heat and mass exchange mechanisms during the HDH process [14]. However, the adoption of specialized solar collector contributes to a significant increase in the capital cost of the overall system, thereby causing a substantial increase in the cost of freshwater production [15]. In the case of the waste heat energy-powered HDH process, a hybrid system utilizes the waste heat of an operational pre-existing unit [16]. The waste heat rejected in the form of hot dry air is either employed to indirectly preheat the air/water [17] or directly adopted as process air [18]. It has been determined that the extraction of waste heat reduces its environmental impact and significantly contributes to the improvement of the pre-existing unit's performance owing to effective heat rejection [19]. Unlike centralized desalination systems that utilize thermal power plant's medium (100 °C–400 °C) and high (> 400 °C) temperature waste heat [20,21], decentralized freshwater production adopts low-grade waste heat (< 100 °C) recovered from heat, ventilation, and air conditioning (HVAC) units [22] and solar photovoltaic (PV) [23] panels. It is noteworthy that low-grade waste heat-powered HDH desalination systems have been gaining momentum only during the recent past owing to the high demand worldwide for both electricity and water. A few theoretical/mathematical studies have been conducted on HDH desalination systems powered by HVAC [22,24–27] and PV panel [28,29] waste heat. However, the results would differ significantly during actual operation owing to the thermal loss and transient behavior. A limited number of experimental research works on low-grade waste heat-powered HDH desalination systems have also been reported. These are discussed below.

Xu et al. [30] carried out an experimental optimization study on a hybrid heat pump–HDH desalination system assisted by a solar collector. The effects of the water and air flow rates, their mixing ratio, and the thermodynamic behavior on the system performance were evaluated by adopting honeycomb cellulose packing material. A maximum freshwater productivity of approximately 12.38 kg/kWh was achieved by the hybrid system. The authors concluded that the HDH effect across the humidifier and dehumidifier units can be maximized at a certain optimum mass flow rates of water and air. These were determined to be approximately 0.3 m^3/h and 450 m^3/h, respectively, for the above-mentioned system. Xu et al. [31] further extended the experimentation by incorporating polyhedron plastic ball humidifiers along with residual heat recovery. A similar optimization study indicated that the mass flow rate of preheated seawater across the humidifier had a greater influence on the gained output ratio (GOR) compared with that on freshwater productivity. Furthermore, the performance of the cellulose humidifier in terms of humidification efficiency was 27.76% higher than that of the polyhedron plastic ball owing to the former's improved wet surface area. Shafii et al. [32] attempted a novel investigation on a hybrid HDH system that directly utilized the condenser reject air of a heat pump as process air for the HDH unit. A cellulose pad was adopted as the humidifier material. An optimization study involving evaluation of the effects of water mass flow rate, air volume flow rate, and ambient air temperature on the system performance was conducted. The results indicated that a maximum freshwater productivity of 2.79 kg/h was achieved with an increase in the relative humidity and air volume flow rate across the dehumidifier section. The system's GOR was identified to decrease with an increase in the ambient air temperature. Similarly, Santosh et al. [33] attempted a simulation and experimental investigation on a novel hybrid HDH–AC system wherein the rejected air of a domestic AC unit's condenser was directly utilized as process air for the HDH system. A season-based analysis indicated that the freshwater productivity and GOR of the hybrid HDH–AC system increased with an increase in the air temperature across the humidifier inlet. This contributed to higher humidification efficiency. The study was extended further to optimize and evaluate the effects of air temperature, humidity ratio, water flow rate, and coolant flow rate while utilizing cellulose and polyvinyl chloride (PVC) humidifier materials [34]. The results indicated that improved freshwater productivity of 7.1 kg/h was achieved for optimum water flow rates of 0.5 m^3/h and 0.9 m^3/h across the humidifier and dehumidifier units, respectively.

Considering the HDH system powered by a PV panel waste heat, Wang et al. [35] carried out theoretical and experimental studies on the utilization of PV panel Tedlar surface waste heat for producing freshwater by the HDH technique. An optimization study to evaluate the effect of water temperature on the evaporation and condensation mass flow rates was conducted with PVC packed bed humidifier. The authors reported that these two parameters improved with an increase in the water evaporative temperature and a decrease in the coolant temperature, respectively. A maximum freshwater productivity of 0.873 kg/m^2/day was achieved by the above system. Similarly, Gabrielli et al. [23] carried out an optimal design analysis of a hybrid HDH–PV thermal (PVT) module with the optimization of the temperature and the mass flow rates of water and air across the various sections of the system. The results indicated that an increase in water mass flow rate across the PVT module caused an increase in the heat extraction rate. This subsequently increased the water preheated temperature and freshwater productivity (0.21 kg/h.m^2) of the HDH system.

Thus, from the present perspective, it is evident that the research involving experimental evaluation of the performance of a hybrid HDH desalination system powered by low-grade waste heat (< 100 °C) is limited. Furthermore, most studies adopted a single humidifier material and performed limited analysis on the influence of process parameters. However, the structure/characteristics of the humidifier material and optimized conditions have a predominant influence on the HDH system performance [36–38]. It is noteworthy that in addition to the utilization of individual feed channels across the humidifier and dehumidifier, the analyses were limited to the optimization of the feed/air flow rates. Additionally, all the reported works employed coolant (seawater/refrigerant) at temperatures of ≤18 °C across the dehumidifier that aids in freshwater production during dehumidification, at the cost of the coolant temperature. However, achieving this coolant temperature range is a difficult task in remote areas across the globe that lack access to proper electricity and is dependent on decentralized desalination technology for satisfying the potable water requirements. It is worth mentioning that two-thirds of the global rural population that lack

access to drinking water also lack access to electricity [39]. Therefore, the present work focuses on the direct utilization of seawater (25 °C) as coolant across the dehumidifier without any precooling mechanism, along with the process of coolant initially being preheated by the latent heat recovery from the humidified air through interconnected feed flow across the humidifier and dehumidifier units. Further, in addition to the optimization of air/feed flow rates, the system's maximum productivity is evaluated considering the temperature of air/feed across the humidifier unit. To evaluate the effect of the physical characteristics of the humidifier, comparative investigation considering different humidifier packing materials such as tri-pack ring (TPR), small pall ring (SPR; diameter = 16 mm), large pall ring (LPR; diameter = 25 mm), super intalox saddle ring (ISR), and snowflake ring (SFR) is carried out for the optimized conditions. Thus, the major objectives of the present work include the following: (i) to evaluate the effect of direct utilization of seawater across the dehumidifier of low-grade waste heat powered HDH desalination system, (ii) optimize the operating conditions for maximizing the humidification and dehumidification effectiveness in conjunction with different packed humidifiers, and (iii) analyze the quality of freshwater produced for the potable purpose.

2. System description

The schematic layout and a photographic image of the low-grade waste heat-powered HDH desalination system are depicted in Fig. 1 and Fig. 2, respectively. The major components of the HDH experimental set-up include a humidifier unit (L × W × H = 13 × 13 × 33 cm) loaded with the packing material, finned tube heat exchange (FTHE) dehumidifier unit (L × W × H = 13 × 13 × 33 cm), air blower (B1) for air circulation, water pump (P1) for feed circulation, and waste heat energy simulator-cum-regulator (heat exchanger-based electric heating unit). The overall HDH system performance was evaluated comparatively by adopting different humidifier packing materials, including tri-pack, pall rings (diameter = 16 mm and 25 mm), saddle ring, and snowflake. The unit was loaded with a random packing material that aids in an effective humidification process owing to the improved wet surface area interaction. Plastic PVC-based packing material was considered due to its cost-effectiveness and non-corrosive characteristics during its interaction with seawater. It is noteworthy that approximately 96% of cooling tower applications adopt PVC plastic owing to their material-based advantages such as homogeneous thickness, high structural/thermal stability, reliable chemical resistance, and improved lifetime. A comparative analysis was performed with random packing's of TPR, SPR (diameter = 16 mm), LPR (diameter = 25 mm), ISR, and SFR humidifiers in the humidifier unit as shown in Fig. 3. These packing materials have been adopted extensively in gas-liquid interaction systems owing to their effectiveness in the efficient heat and mass transfer (HMT) process [40]. The significant structural parameters of these materials are listed in Table 1. The packing materials aid in the effective interaction of hot dry air with uniformly sprayed seawater across the humidifier chamber with the aid of a water distribution channel (Fig. 2). The feed utilized in the present investigation was seawater collected from the East Sea coast in the Republic of Korea. The humidifier and dehumidifier units were fabricated with identical dimensions to maximize the HDH effect through efficient surface area interaction between feed and air across both the units. The dehumidifier FTHE consisted of

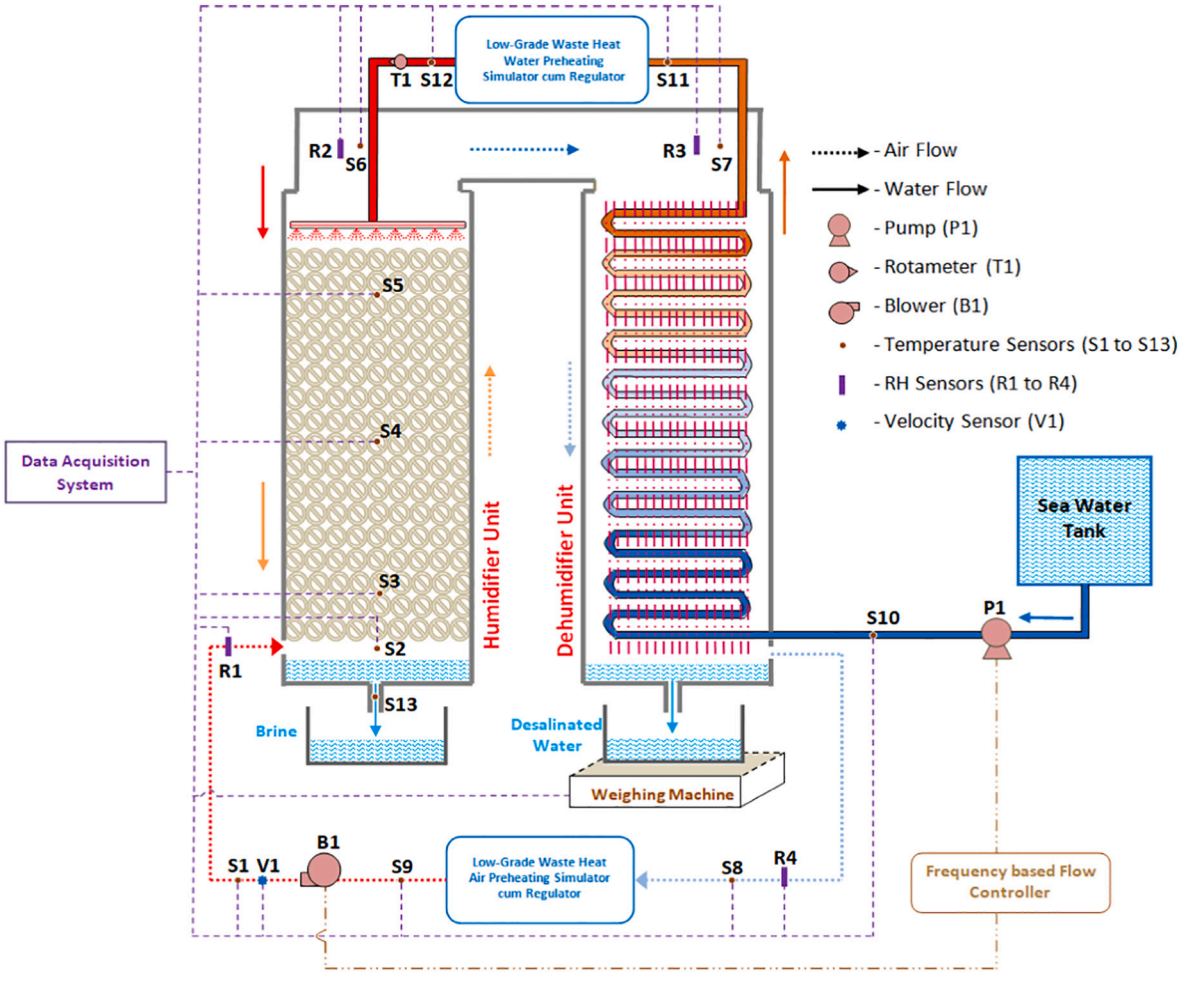

Fig. 1. Schematic diagram of low-grade waste heat-powered HDH desalination system.

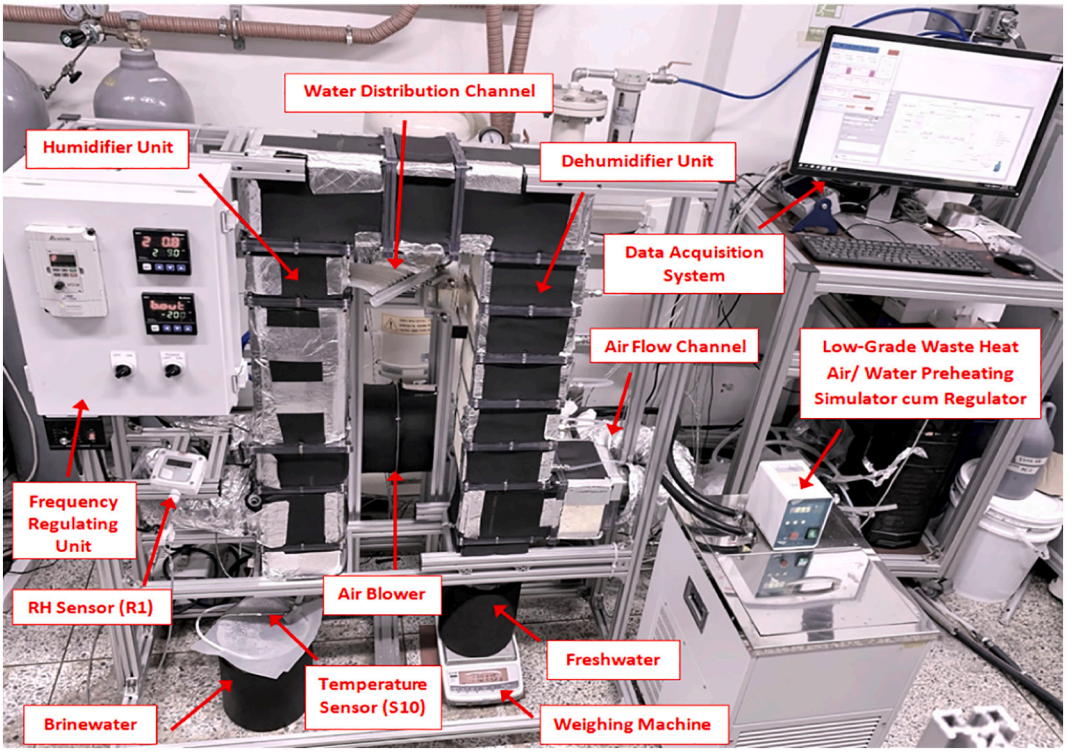

Fig. 2. Photographic view of the experimental set-up.

Fig. 3. Humidifier unit loaded with random packing of (a) tri-pack rings, (b) small pall rings, (c) large pall rings, (d) super intalox saddle rings, and (e) snow-flake rings.

Table 1
significant structural detail of humidifier packing materials.

Humidifier material	Ring diameter (mm)	Height (mm)	Thickness (mm)	Specific surface area (m^2/m^3)	Void fraction (%)	Packing factor (m^{-1})	Number of packing units inside humidifier
Tri-pack ring (TPR)	25	25	1	190	92	–	480
Small pall ring (SPR)	16	16	1.1	188	91	249	1000
Large pall ring (LPR)	25	25	1.2	175	90	239	280
Super intalox saddle ring (ISR)	50	25	1.5	168	68	184	250
Snowflake ring (SFR)	94	34	1.5	138	97	–	25

transverse fins made of aluminum mounted over the copper tubes for an effective dehumidification process. The freshwater productivity was monitored constantly using a weighing machine at the bottom of the dehumidifier unit. In addition, the entire system was insulated to prevent convective and radiative heat losses to the atmosphere.

3. Experimentation

The experimentation focused on the utilization of low-grade waste heat energy acquired from the HVAC systems and PV panels (temperature of <100 °C) for preheating the air and feed across the HDH system. Therefore, considering the set-up's constituent material (polycarbonate plastic) and operational constraints of the instrumentation, preheating temperatures in the ranges 50–70 °C and 45–55 °C were considered for air and feed, respectively. Furthermore, owing to the high thermal efficiency of a closed-air circulation compared to open-air circulation [14,41], the former mechanism was considered in the present work with the utilization of an airflow channel arrangement as shown in Fig. 2. The experimentation focused on the initial optimization of the feed mass flow rate ($\dot{m}_w$) considering an initial air preheating temperature (T_a) of 60 °C at the humidifier inlet. This was followed by optimization of the air mass flow rate ($\dot{m}_a$). Furthermore, based on the optimized mass flow rates of feed and air, the performance of the HDH system was evaluated with only the low-grade waste heat-powered air preheating process (T_a = 50–70 °C). Finally, for the optimized mass flow rates (of feed and air) and air preheating temperature, the system was evaluated with an additional feed preheating process (T_w = 45–55 °C). Thus, the set-up functioned as a dual-fluid preheated HDH system. In addition, to evaluate the effect of preheating on the performance of the developed HDH unit, a comparative evaluation based on the optimized conditions was performed with only-air preheating and the dual-fluid preheating process, to identify the preheating technique that contributed better toward productivity maximization. Thus, the entire study focused on the optimization of process parameters, humidifier materials, and preheating techniques with the utilization of low-grade waste heat to maximize the HDH efficiency for the conversion of seawater to freshwater.

The experimental procedure involved initial preheating of the air to the desired temperature to achieve the low-grade waste heat condition. The hot dry air was allowed to flow through the humidifier unit. Upon interaction, the hot dry air was humidified, which caused a decrease in its temperature and an increase in its relative humidity (RH), and further the hot humidified air reached the FTHE dehumidifier unit. It is noteworthy that seawater at 25 °C was directly utilized as the coolant across the dehumidifier unit considering its instantaneous usage for the dehumidification process without any auxiliary cooling mechanism even during summer [42]. The interaction between the coolant and humidified hot air at the dehumidifier unit resulted in the production of freshwater owing to the condensation or latent heat extraction from the humidified air. The dehumidified air at the exit of the dehumidifier unit was re-circulated for the subsequent cycle of operation. Thus, the airflow was a closed cycle process. The brine and freshwater were collected at the bottom of the humidifier and dehumidifier units, respectively. Thus, the present system operated through a closed-air open-water cycle mechanism. However, it is also to be noted that the feed passes through the dehumidifier tubes during its flow from the seawater tank toward the humidifier unit. This aids in the dual process of the extraction of the latent heat of condensation on the surface of the tubes and the simultaneous preheating of the feed flowing inside the tubes. All the experiments were carried out after the system attained a steady-state condition.

4. Measurement and instrumentation

The various temperatures and RH parameters of air were measured across different locations of the HDH set-up during the experiment (Fig. 1). The temperature of the hot dry air across the blower's entry and exit (S9 and S1, respectively) and humidifier's entry (S2), humidified air across the humidifier unit (S3–S6) and dehumidifier's entry (S7), and dehumidified air at the dehumidifier's exit (S8) were measured using temperature probe sensors of accuracy ±0.1%. Similar sensors were adopted for measuring the feed temperature inside the tube of the dehumidifier unit and brine (S10–S13). The RH of the process air at the entries and exits of the humidifier (R1 and R2, respectively) and dehumidifier (R3 and R4) units were measured with the aid of an HX92B Omega RH transmitter (accuracy = ±2.5%). Furthermore, the KIMO CTV110 air velocity transmitter (V1; accuracy = ±3%) was utilized to measure the air velocity. The freshwater productivity of the system was monitored constantly using an electronic weighing balance (Type: CUW6200HX; accuracy = ±1%). All these sensors and instruments were calibrated prior to usage and connected to a customized data acquisition system for constant monitoring and recording of the data at regular intervals of 2 s. The air and feed flow across the HDH system were circulated using a frequency-regulated air blower (164 W) and micro water pump (maximum revolution speed = 5500 rpm), respectively. Furthermore, the feed flow rate was monitored constantly using a rotameter (T1 in Fig. 1).

To evaluate the desalination effectiveness, water quality analysis was carried out for both seawater and the freshwater produced by the present HDH system. The physical properties including pH, salinity, total dissolved solids (TDS), and electrical conductivity (EC) were analyzed in detail. Furthermore, the chemical quality analysis involved the measurement of the major constitutional ions including Na^+, Mg^{2+}, Ca^{2+}, K^+, and Sr^+ as well as other minor cations and anions. The analysis was performed immediately after the production of freshwater to prevent contamination, which can contribute to flawed results.

5. Performance evaluation factors

The various factors that aid in the performance analysis of the developed low-grade waste heat-powered HDH desalination system are discussed in this section.

5.1. Waste-heat recovery potential factor

The capability of the HDH system to utilize the low-grade waste heat energy to efficiently convert seawater into freshwater (expressed as the system's waste-heat recovery potential) can be evaluated in terms of the gained output ratio (*GOR*):

$$WPF\ (or)\ GOR = \frac{Y\gamma}{Q_{in}} \tag{1}$$

where Y, γ, and Q_{in} represent the yield, latent heat of condensation, and

low-grade waste heat input to the HDH system.

5.2. Humidifier performance potential factor

Based on the characteristics of the air across the humidifier unit when the different humidifier packing materials are used, the humidifier material's thermal performance potential could be evaluated in terms of the humidification performance potential factor (*HPF*). The *HPF*s of the different humidifier packing materials can be determined as follows [43]:

$$HPF_i = \frac{\dot{m}_a\left(\omega_{a,humid\ out} - \omega_{a,humid\ in}\right)L}{Q_{in}} \tag{2}$$

where i represent TPR, SPR, LPR, ISR, and SFR, respectively. Furthermore, $\dot{m}_a$ is the mass flow rate of air across the HDH system; $\omega_{a,humid\ out}$ and $\omega_{a,humid\ in}$ are the humidity ratios of the air medium across the exit and entry, respectively, of the packed bed humidifier unit; and L represents the latent heat of feed.

The heat energy input to the humidifier unit, Q_{in}, can be determined as

$$Q_{in} = \dot{m}_a\left(h_{a,preheat\ out} - h_{a,preheat\ in}\right) + \dot{m}_w C_{pw}\left(T_{w,preheat\ out} - T_{w,preheat\ in}\right) \tag{3}$$

where $\dot{m}_w$ and C_{pw} indicate the mass flow rate and specific heat, respectively, of the feed across the HDH unit. $h_{a,preheat\ out}$ and $h_{a,preheat\ in}$ represent the enthalpy of air after and before the preheating process, respectively. Similarly, $T_{w,preheat\ out}$ and $T_{w,preheat\ in}$ are the temperatures of the feed after and before the preheating process, respectively. In the present study, $T_{w,preheat\ out} = T_{w,humid\ in}$. Here, $T_{w,humid\ in}$ represents the temperature of the feed across the humidifier inlet, and $\dot{m}_w C_{pw}\left(T_{w,preheat\ out} - T_{w,preheat\ in}\right)$ is equal to zero in the case with only the air preheating process.

5.3. Humidification effectiveness factor

The effectiveness of the humidification process with the adoption of the different humidifier materials could be evaluated in terms of the humidification effectiveness factor. It accounts for the humidity ratio of the air across the humidifier unit. Thus, the humidification effectiveness factor (ε) is calculated by [12].

$$\varepsilon_i = \frac{\omega_{a,humid\ out} - \omega_{a,humid\ in}}{\omega_{a,humid\ out,s} - \omega_{a,humid\ in}} \tag{4}$$

where ε represent the humidification effectiveness across the humidifier unit of the present HDH system when TPR, SPR, LPR, ISR, and SFR, respectively, are applied. Furthermore, $\omega_{a,humid\ out,s}$ is the humidity ratio when the humidified air at the exit of the humidifier unit is saturated.

5.4. Heat capacity ratio factor

Humidification involves HMT mechanisms. Thereby, the humidity ratio of air varies with the variation in the humidifier packing material. The humidity ratio across the humidifier unit plays a major role in the enthalpy of the humidified air, which is expressed in terms of the heat capacity ratio factor (*HCF*):

$$HCF_i = \frac{\Delta\dot{H}_{feed,max}}{\Delta\dot{H}_{air,max}} \tag{5}$$

Table 2
Details of instruments, including error and standard uncertainty.

Instruments utilized	Parameters measured	Instrumental range	Accuracy	Standard uncertainty
Temperature probe sensor	Temperature	−200–850 °C	±0.1%	0.1 °C
HX92B Omega RH transmitter	Relative humidity	0–100%	±2.5%	0.1%
KIMO CTV110 air velocity transmitter	Air Velocity	0–30 m/s	±3%	0.01 m/s
LF 101 rotameter	Mass flow of feed	0–2 L/min	±2%	0.1 L/min
Electronic weighing balance	Yield quantity	0–6200 g	±0.01%	0.01 g

where $\Delta\dot{H}_{feed,max}$ and $\Delta\dot{H}_{air,max}$ are the maximum differences in the total enthalpy rate of the cold feed side and hot airside, respectively [34]:

$$\Delta\dot{H}_{feed,max} = \dot{m}_w C_{pw}\left(T_{a,humid\ in} - T_{w,humid\ in}\right) \tag{6}$$

$$\Delta\dot{H}_{air,max} = \dot{m}_a C_{pa}\left(T_{a,humid\ in} - T_{w,humid\ in}\right) \tag{7}$$

where C_{pa} and $T_{a,humid\ in}$ indicate the specific heat of the air and its temperature across the humidifier inlet, respectively.

6. Uncertainty and error analysis

Error and uncertainty analyses were carried out to evaluate the instrumentation errors, errors in the measured parameter, and experimental uncertainty. The maximum possible error in the instruments utilized and the recorded parameters were calculated as the root sum square of the fixed instrumental error and measured random error as listed in Table 2 [44]. Furthermore, the uncertainty in the experimentally measured individual parameters and its resultant data was evaluated by the Kline and McClintock uncertainty technique [45]:

$$R = R\left(P_1, P_2, P_3, P_4, P_5 \ldots, P_n\right) \tag{8}$$

where R is the resultant defined as a function of n independent parameters (P_1, P_2, P_3, P_4, P_5…, P_n).

Thus, the percentage of uncertainty in the resultant is denoted as U_R. It can be determined using the uncertainties in the individual parameters (ΔP_1, ΔP_2, ΔP_3…, ΔP_n) by

$$U_R = \sqrt{\left(\frac{\partial R}{\partial P_1}\Delta P_1\right)^2 + \left(\frac{\partial R}{\partial P_2}\Delta P_2\right)^2 + \left(\frac{\partial R}{\partial P_3}\Delta P_3\right)^2 + \ldots\ldots + \left(\frac{\partial R}{\partial P_n}\Delta P_n\right)^2} \tag{9}$$

For example, the uncertainty in the humidification performance potential factor (Eq. 2, where $\dot{m}_a$ and L are constants) is accounted for based on the uncertainties in the independently varying parameters that include $\omega_{a,humid\ out}$, $\omega_{a,humid\ in}$, and Q_{in}. Thus, *HPF* is a function of the above three parameters as follows:

$$HPF = f\left(\omega_{a,humid\ out}, \omega_{a,humid\ in}, Q_{in}\right) \tag{10}$$

Therefore, the percentage of uncertainty in the *HPF* (U_{HPF}) is determined as

$$U_{HPF} = \sqrt{\left(\frac{\partial R}{\partial \omega_{a,humid\ out}}\Delta\omega_{a,humid\ out}\right)^2 + \left(\frac{\partial R}{\partial \omega_{a,humid\ in}}\Delta\omega_{a,humid\ in}\right)^2 + \left(\frac{\partial R}{\partial Q_{in}}\Delta Q_{in}\right)^2} \tag{11}$$

Table 3
Experimental uncertainties of various key parameters.

Humidifier packing	U_{HPF}	U_{GOR}	U_{ε}
Tri-pack ring	±2.07%	±1.23%	±2.11%
Small pall ring	±2.09%	±1.25%	±2.13%
Large pall ring	±2.08%	±1.24%	±2.14%
Super intalox saddle ring	±2.05%	±1.22%	±2.12%
Snowflake ring	±2.05%	±1.20%	±2.12%

Similarly, the experimental uncertainties for all the major parameters were calculated and are listed in Table 3.

7. Results and discussion

A series of experiments were carried out to 1) evaluate the potential of low-grade waste heat energy for the conversion of seawater into freshwater through the HDH technique with the direct utilization of coolant (seawater at 25 °C) and 2) optimize the process parameters with identification of the humidifier packing material for maximum freshwater productivity. An initial analysis of the HDH system was performed to achieve the above objectives. It involved the usage of TPR packed humidifier for optimizing the system's water mass flow rate (0.3 to 1.1 L/min), considering air preheated temperature and mass flow rate of 60 °C and 2 kg/min across the humidifier inlet, respectively. The performance analysis was extended further to evaluate the effect of air mass flow rate in the range from 1 kg/min to 3.5 kg/min, for the optimized water mass flow rate. Then, for the optimum flow conditions of water and air that would contribute to the maximum mixing ratio across the humidifier unit, the effect of low-grade waste heat-powered air and water preheating temperatures of 50–70 °C and 45–55 °C, respectively, were analyzed to identify the optimum working temperature of the process fluids for maximizing the HDH efficiency. Subsequently, for the optimized flow and operating temperature conditions across the developed system, a comparative performance analysis was performed with SPR, LPR, ISR, and SFR to identify the humidifier material that would yield the maximum freshwater productivity. Therefore, this section involves a detailed discussion on the optimization of the feed and air flow rates, their operating temperature, and the effect of various humidifier packing materials on the performance of the low-grade waste heat-powered HDH system. It is worth mentioning that prior to the experimentation with preheating of air; a preliminary feasibility analysis without preheating was carried out. However, zero Y was achieved because air at lower temperatures holds lesser water vapor leading to inefficient humidification [46]. Subsequently, during dehumidification, utilization of seawater at 25 °C which was much higher than the dew point temperature of the humidifier air without preheating (~ 13 to 15 °C) contributed to inefficient latent heat recovery leading to zero Y.

7.1. Performance based on feed mass flow rate, $\dot{m}_w$

The characteristic variation in the temperature and RH across the humidifier and dehumidifier units of the developed HDH system and its effect on the humidity ratio variations and freshwater yield is shown in Fig. 4. As mentioned earlier, the waste heat preheating temperature of the air was initially maintained at 60 °C with a mass flow rate of 2 kg/min. The mass flow rate of the feed, $\dot{m}_w$, was varied between 0.3 and 1.1 L/min to identify the optimum $\dot{m}_w$ that contributes to the maximum heat and mass transfer across both humidifier (loaded with TRP packed humidifier) and dehumidifier units and thereby, maximizing the yield. Fig. 4(a) shows that the temperature reduction ($\Delta T_{a,humid}$) and RH increment ($\Delta RH_{a,humid}$) of the air across the humidifier unit increased with an increase in the $\dot{m}_w$ across the HDH system. The minimum $\Delta T_{a,humid}$ and $\Delta RH_{a,humid}$ of approximately 18.37 °C and 51.69%, respectively, were observed across the humidifier unit for the minimum $\dot{m}_w$ (0.3 L/min). Similarly, the maximum $\Delta T_{a,humid}$ and $\Delta RH_{a,humid}$ of

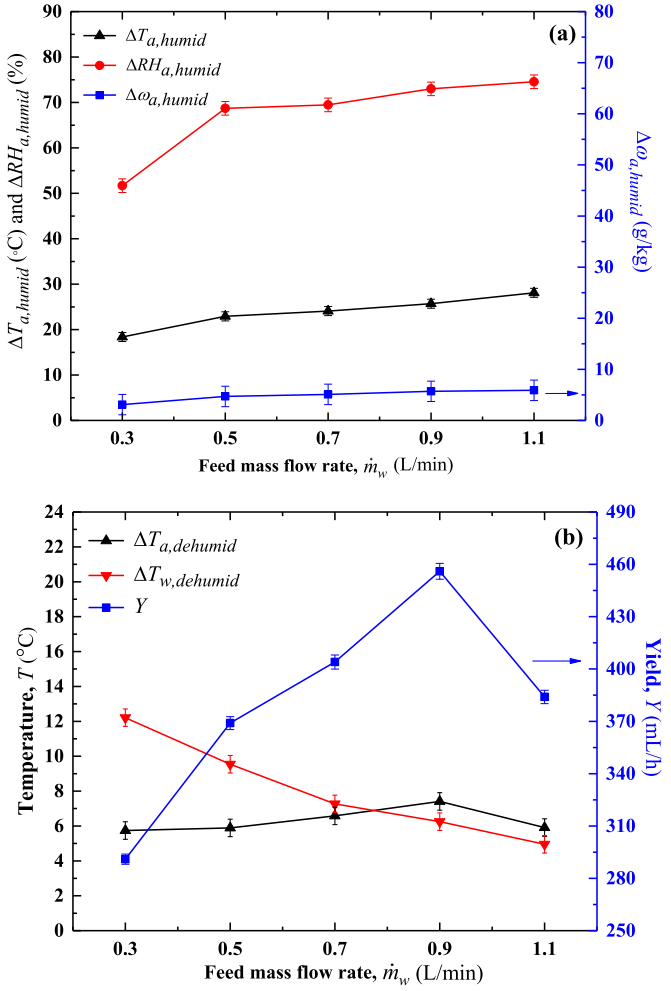

Fig. 4. Characteristic variation across (a) humidifier and (b) dehumidifier units with variation in $\dot{m}_w$ (for $\dot{m}_w$= 0.9 L/min and $\dot{m}_a$= 3.5 kg/min).

28.07 °C and 74.55% were observed for the maximum $\dot{m}_w$ (1.1 L/min). The above variation in the temperature and RH of the air contributed to the minimum and maximum increase in the humidity ratio across the humidifier unit ($\Delta\omega_{a,humid}$) of approximately 3.1 and 5.9 g/kg, for $\dot{m}_w$ of 0.3 and 1.1 L/min, respectively (Fig. 4(a)). It can be observed that the $\Delta T_{a,humid}$, $\Delta RH_{a,humid}$, and $\Delta\omega_{a,humid}$ across the humidifier unit increased with an increase in the $\dot{m}_w$ across the HDH unit. The maximum difference between the temperature reduction and RH increase in the case of $\dot{m}_w$ with 1.1 L/min could be attributed to the higher moisture gain or evaporation of water when the hot dry air interacted with the feed. It is noteworthy that there exists an optimum mixing ratio between air and water across the humidifier unit for maximum HMT to occur. This optimum mixing ratio contributes to the maximum decrease in temperature of the humidified air ($T_{a,humid\ out}$) as well as the maximum increase in its RH ($RH_{a,humid\ out}$). These collectively result in a higher $\omega_{a,humid\ out}$ across the humidifier exit. A similar trend was observed by Xu et al. when a cellulose-packed humidifier was used [30]. It is also to be noted that this phenomenon is system-specific and also depends on other parameters such as the type of humidifier material adopted and characteristics of the air and water across the humidifier unit [31,34].

The variation in hourly freshwater yield (Y) with an increase in $\dot{m}_w$ and the corresponding characteristics of the air and feed across the dehumidifier unit are shown in Fig. 4(b). Seawater at a temperature of 25 °C was utilized directly as a coolant across the dehumidifier unit for the dehumidification process without precooling mechanism. It can be observed that with an increase in $\dot{m}_w$ from 0.3 to 0.9 L/min, the

temperature reduction of air ($\Delta T_{a,dehumid}$) and temperature increase of water ($\Delta T_{w,dehumid}$) across the dehumidifier unit showed increasing and decreasing trends, respectively. The minimum decrease in air temperature (5.74 °C) in conjunction with the maximum increase in feed temperature (12.21 °C) across the dehumidifier unit was identified for the lower $\dot{m}_w$ of 0.3 L/min. Similarly, the maximum decrease in air temperature and minimum increase in feed temperature of approximately 7.41 and 6.25 °C were observed when $\dot{m}_w$ was maintained at 0.9 L/min. However, the hourly Y displayed an increasing trend. It attained a minimum of 291 mL/h and a maximum of 456 mL/h for $\dot{m}_w$ of 0.3 and 0.9 L/min, respectively. This is because the increase in the temperature of the coolant (seawater) during its interaction with the humidified air reduced with an increase in the $\dot{m}_w$ across the dehumidifier inlet (Fig. 4 (b)). This sustained a lower temperature across the tube surface of the FTHE unit. Subsequently, the humidified air in contact with the surface of the tubes experienced an enhanced temperature decrease, which contributed to improving the condensation process and Y. The temperature of the process air also decreased owing to the higher rate of condensation. Thereby, $\Delta T_{a,dehumid}$ was higher for the higher $\dot{m}_w$ of 0.9 L/min. However, in addition to the comparatively lower inlet humidified air temperature across dehumidifier inlet, the time of contact between the humidified air and coolant reduced with an increase in $\dot{m}_w$ beyond 0.9 L/min to 1.1 L/min. This collectively contributed to the condition wherein the air did not achieve the saturation point required for an effective condensation process. The ineffective or partial condensation contributed to a lower $\Delta T_{w,dehumid}$, and lower $\Delta T_{a,dehumid}$ along with a comparatively lesser Y of 384 mL/h. Thus, a higher Y could be achieved when the $\dot{m}_w$ across the HDH system was maintained at 0.9 L/min. It is noteworthy that although effective humidification was achieved with a $\dot{m}_w$ of 1.1 L/min, the effect of contact time reduction and comparatively lower humidified air temperature contributed to a lesser Y during dehumidification. This provides insight that there exists individual optimum $\dot{m}_w$ across the humidifier and dehumidifier units to achieve effective humidification and dehumidification processes, respectively. This can be considered as a limitation in the case of low-grade waste heat-powered HDH systems with interconnected feed flow across the dehumidifier and humidifier units.

7.2. Performance based on variation in air mass flow rate, $\dot{m}_a$

The characteristic variations in the key parameters across the humidifier and dehumidifier units with an increase in the air mass flow rate ($\dot{m}_a$) across the HDH system for the optimum $\dot{m}_w$ of 0.9 L/min are shown in Fig. 5. It can be observed that the temperature of the humidified air ($T_{a,humid\ out}$) increased with an increase in $\dot{m}_a$ from 1.5 to 3.5 kg/min. As the temperature and RH are inversely dependent parameters, the RH of the humidified air ($RH_{a,humid\ out}$) was observed to exhibit a decreasing trend with an increase in $\dot{m}_a$. However, the maximum increase in $\Delta\omega_{a,humid}$ of approximately 7.8 g/kg was observed when $\dot{m}_a$ was 3.5 kg/min. $\Delta\omega_{a,humid}$ also displayed an increasing trend with an increase in $\dot{m}_a$ (see Fig. 5(a)). This subsequently resulted in the production of a higher Y of approximately 737 mL/h during dehumidification (Fig. 5(b)). As evident from Fig. 5(b), both the operating fluids displayed an increasing trend (indicating an efficient temperature reduction of air and a temperature increase in the water) with an increase in $\dot{m}_a$ from 1.5 to 3.5 kg/min. This signifies the potential of $\dot{m}_a$ to contribute to the efficiency of the dehumidification process. The heat transfer rate across the tubes of the dehumidifier unit increased with an increase in $\dot{m}_a$ from 1.5 to 3.5 kg/min. This contributed to a higher $\Delta T_{w,dehumid}$. The minimum and maximum increases in water temperature ($\Delta T_{w,dehumid}$) across the dehumidifier unit were approximately 5.1 and 11.9 °C for $\dot{m}_a$ of 1.5 and 3.5 kg/min, respectively. This preheated feed when subsequently sprayed across the humidifier unit increased the humidity ratio of the hot dry air and, thereby, contributed to a higher $\Delta\omega_{a,humid}$ for a higher $\dot{m}_a$. This substantiated the results obtained in Fig. 5(a). Thus, $\dot{m}_a$ was observed to predominantly influence the dehumidification rate across

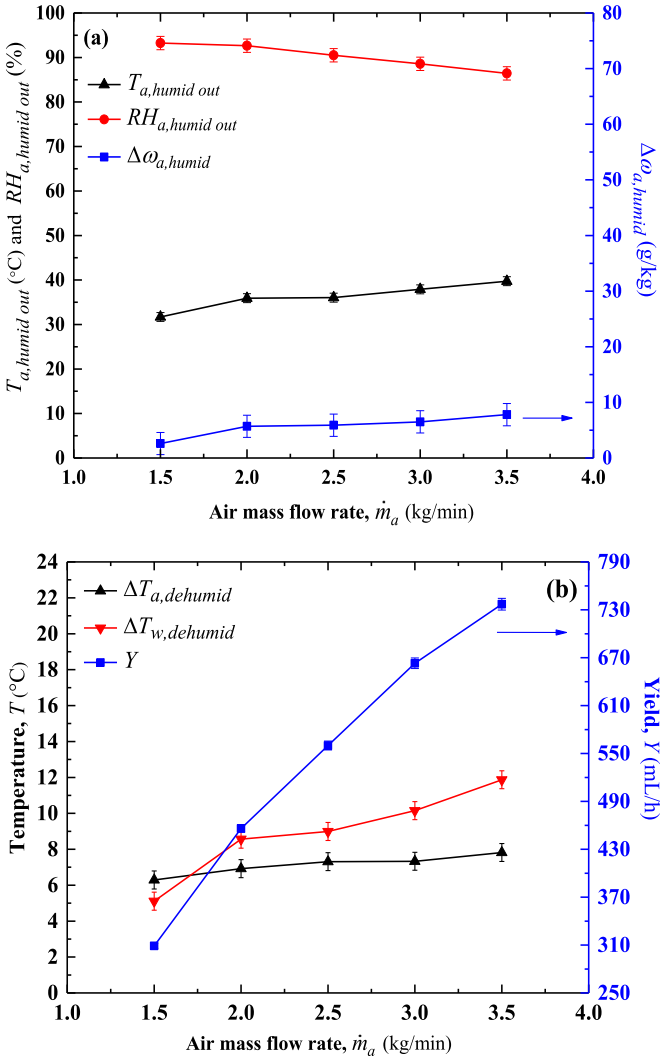

Fig. 5. Characteristic variation across (a) humidifier and (b) dehumidifier units with variation in $\dot{m}_a$ (for $\dot{m}_w$= 0.9 L/min).

Fig. 6. Photograph of humidified air condensation across the surface of the humidifier exit with $\dot{m}_a$ of 1 kg/min.

the FTHE and subsequently, the temperatures of the air and water mediums across the HDH system. It was also observed during the experiment that for a least $\dot{m}_a$ of 1 kg/min, though effective humidification of air occurred across the humidifier (see Fig. 6); its magnitude was insufficient for efficient interaction with the coolant across the dehumidifier. Therefore, zero Y was achieved from the present low-grade waste heat-powered HDH system with a $\dot{m}_a$ of 1 kg/min.

7.3. Influence of air temperature across humidifier inlet, $T_{a,humid\ in}$

Considering the feasibility and operation of the developed HDH system within the temperature range of the low-grade waste heat energy, the system's performance was evaluated for a temperature of 50–70 °C with the optimum $\dot{m}_w$ and $\dot{m}_a$ of 0.9 L/min and 3.5 kg/min, respectively. The variation in the key parameters across the humidifier and dehumidifier units during the experiment is depicted in Fig. 7. The rate of temperature reduction and RH increase in air across the humidifier unit increased with an increase in $T_{a,humid\ in}$. This contributed to the increasing trend of $\Delta T_{a,humid}$ and $\Delta RH_{a,humid}$, respectively. The minimum temperature reduction (13.9 °C) and RH increase (53.73%) occurred when the system operated with a $T_{a,humid\ in}$ of 50 °C. Meanwhile, the maximum temperature reduction and RH increase of 25.45 °C and 66.14%, respectively, occurred for a $T_{a,humid\ in}$ of 70 °C. This can be attributed to the better evaporation of the water particles on interaction with the higher-temperature air medium (70 °C), which subsequently resulted in an improved HMT mechanism and thereby, contributed to a higher RH of the humidified air. Consequently, the higher RH contributed to the maximum temperature reduction across the humidifier exit. Thus, an improved $\Delta\omega_{a,humid}$ of 12.4 g/kg was achieved for a $T_{a,humid\ in}$ of 70 °C. For the dehumidifier, increasing trends were observed for $\Delta T_{a,dehumid}$ and $\Delta T_{w,dehumid}$ with maximum increases in temperature of approximately 8.6 °C and 15.6 °C for the operation of the HDH system with a $T_{a,humid\ in}$ of 70 °C. Furthermore, because Y is based on the characteristics of $\omega_{a,humid\ out}$ across the humidifier unit, lower and higher Y of 527 mL/h and 929 mL/h, respectively, were achieved when the HDH system operated with a $T_{a,humid\ in}$ of 50 and 70 °C, respectively. It is also noteworthy that because the HDH system in the present work involves a closed air-circulation technique, a comparatively higher $T_{a,humid\ in}$ contributed to a higher $T_{a,humid\ out}$. Subsequently, during its interaction over the surface of the FTHE, higher heat transfer occurs, which results in the higher exit temperature of the feed water across the dehumidifier outlet ($T_{w,dehumid\ out}$). Consequently, an enhanced rate of evaporation is achieved compared with a lower $T_{a,humid\ in}$ when this water is sprayed across the humidifier unit. This contributes to an improved humidification effect and subsequently, higher Y during dehumidification (evident from Fig. 7(a) and (b)). Therefore, a $T_{a,humid\ in}$ of 70 °C was identified to be the optimum value for the present HDH set-up.

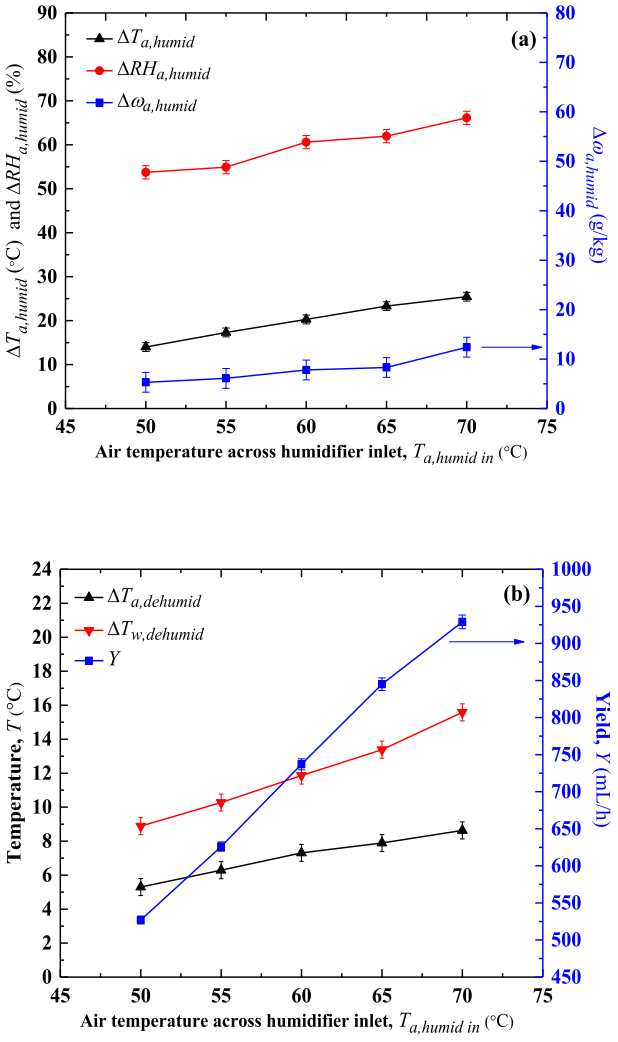

Fig. 7. Characteristic variation across (a) humidifier and (b) dehumidifier units with variation in $T_{a,humid\ in}$.

7.4. Effect of feed temperature across humidifier inlet, $T_{w,humid\ in}$

From the above results, it is apparent that the temperature of the feed across the humidifier inlet ($T_{w,humid\ in}$) plays a significant role in the humidification efficiency and consequently, in the determination of the Y of the entire system. Considering this, the experiment was extended further to evaluate the performance of the developed HDH system with variation in $T_{w,humid\ in}$. In addition to the utilization of the low-grade waste heat energy for preheating the air, the case of feed preheating was considered. It can contribute to a higher rate of humidification and improve the overall system efficiency because air and feed water are preheated simultaneously for the HDH process [14]. Taking into account the configuration of the developed HDH system and operational limitations experienced during the usage of auxiliary measuring devices, a feed preheating temperature across the humidifier inlet in the range of 45 to 55 °C was considered for evaluation. Fig. 8 shows the characteristics of air and feed water across the humidifier and dehumidifier units with an increase in $T_{w,humid\ in}$. The $T_{a,humid\ out}$ and $RH_{a,humid\ out}$ displayed increasing trends with the increase in $T_{w,humid\ in}$ (Fig. 8(a)). Although the optimum $T_{a,humid\ in}$ of 70 °C was maintained for all the cases, the increase in $T_{w,humid\ in}$ from 45 to 55 °C contributed to an increase in the $T_{a,humid\ out}$ across the humidifier exit during the interaction between air and the higher-temperature feed. Furthermore, the higher heat capacity of the feed water with an increase in its temperature ($T_{w,humid\ in}$) resulted in a higher humidification rate, which, in turn, yielded a higher $RH_{a,humid\ out}$. This subsequently contributed to $\omega_{a,humid\ out}$ of 60.7, 70.1, and 80.4 g/kg for $T_{w,humid\ in}$ of 45, 50, and 55 °C, respectively. Similarly, an increasing trend was identified for $\Delta\omega_{a,humid}$ of 9.1, 11.3, and 14.2 g/kg with an increase in $T_{w,humid\ in}$ (Fig. 8(a)). This indicates the improved humidification efficiency achieved with an increase in the feed preheating temperature. Subsequently, during dehumidification, Y of 1064, 1208, and 1385 mL/h were obtained for the dual-fluid heated cases with $T_{w,humid\ in}$ of 45, 50, and 55 °C, respectively (Fig. 8(b)). Thus, a maximum Y of approximately 1385 mL/h could be achieved using the developed low-grade waste heat-powered HDH system with the TRP-packed humidifier for the optimized $T_{a,humid\ in}$ and $T_{w,humid\ in}$ of 70 °C and 55 °C, respectively. Furthermore, a comparison between Fig. 7(b) and 8(b) reveals that the $\Delta T_{a,dehumid}$ and $\Delta T_{w,dehumid}$ across the dehumidifier with the optimum dual-fluid preheated HDH process were higher than those for all the cases using only-air preheated technique. This is an advantageous feature that contributes to a reduction in the energy required for the feed preheating process.

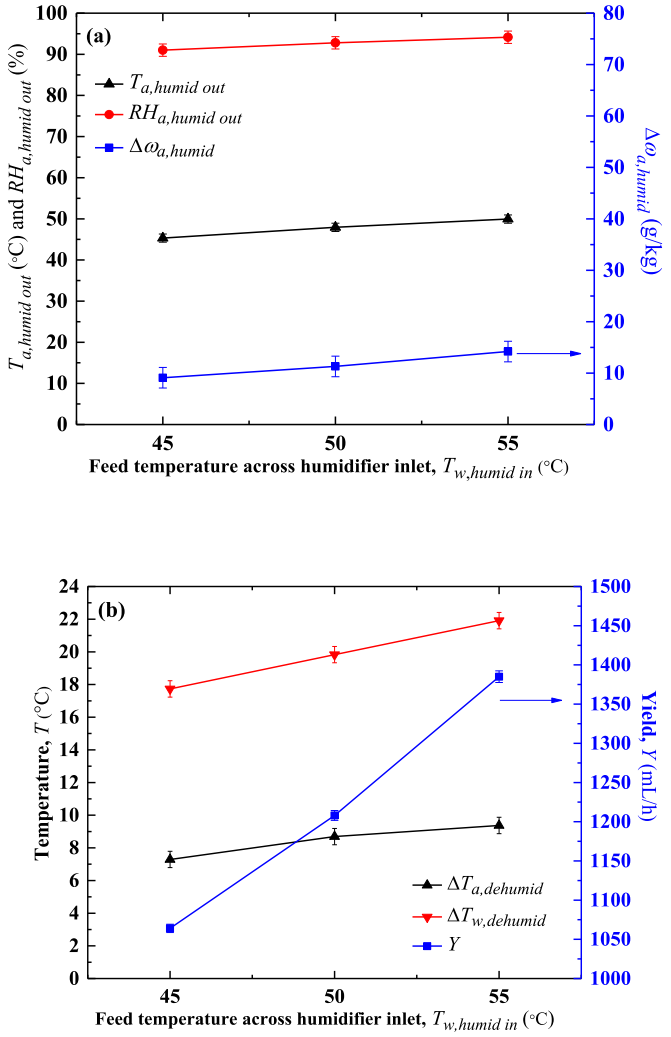

Fig. 8. Characteristic variation across (a) humidifier and (b) dehumidifier units with variation in $T_{w,humid\ in}$(for $\dot{m}_w$= 0.9 L/min, $\dot{m}_a$= 3.5 kg/min, and $T_{a,humid\ in}$ = 70 °C).

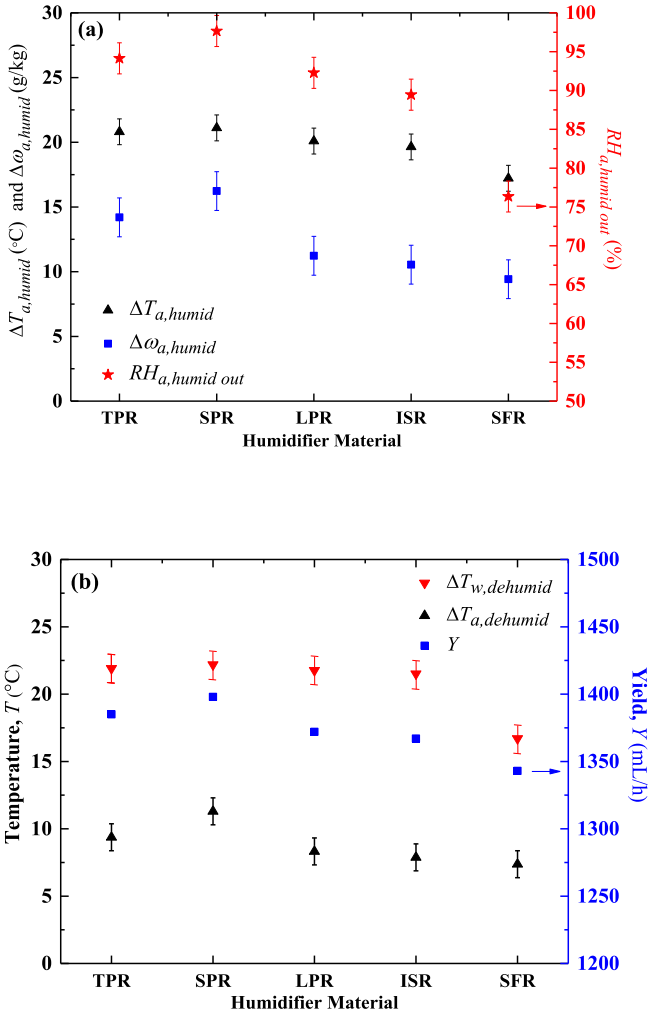

Fig. 9. Characteristic variation across (a) humidifier and (b) dehumidifier units with variation in packed humidifier materials (for $\dot{m}_w$= 0.9 L/min, $\dot{m}_a$= 3.5 kg/min, $T_{a,humid\ in}$ = 70 °C and $T_{w,humid\ in}$ = 55 °C).

7.5. Effect of humidifier packing material

The performance of the low-grade waste heat-powered HDH desalination system with different humidifier packing materials (TPR, SPR, LPR, ISR, and SFR) was evaluated for the optimized conditions of $\dot{m}_w$, $\dot{m}_a$, $T_{a,humid\ in}$, and $T_{w,humid\ in}$ of 0.9 L/min, 3.5 kg/min, 70 °C, and 55 °C, respectively, across the humidifier and dehumidifier units. The effect of the surface area of humidifier packing on the humidification efficiency and overall performance of the system was evaluated. The total surface areas of the TPR, SPR, LPR, ISR, and SFR packing materials in the humidifier unit were 91,200, 188,000, 49,000, 42,000, and 3450 m^2/m^3, respectively. Fig. 9 reveals that the SPR-packed humidifier outperformed the other humidifier packing material across both humidifier and dehumidifier units. The maximum reduction in the temperature of air across the humidifier unit ($\Delta T_{a,humid}$) with the usage of the SPR humidifier was approximately 21.1 °C. Moreover, the maximum RH value ($RH_{a,humid\ out}$) was 97.7%. This indicates the capability of the SPR packing material for an effective humidification process compared with the other humidifiers. The improved humidification efficiency can be attributed to its larger surface area, which facilitates the achievement of an augmented wet surface when feed water flows over it. Thus, an improved evaporation rate of feed water is achieved when the hot dry air and water are in contact with each other on the wet surface area during humidification. This results in the maximum temperature reduction and RH increase of the humidified air medium across the humidifier exit. The mechanism holds true for all the humidifier packing materials considered. Hence, an improved humidification rate (higher $RH_{a,humid\ out}$ with higher $\Delta T_{a,humid}$) is achieved with a packing material having a larger surface area (Fig. 9(a)). Meanwhile, the $RH_{a,humid\ out}$ for TPR, LPR, ISR, and SFR (which have comparatively smaller surface areas) were determined to be approximately 3.6%, 5.5%, 8.4%, and 21.8%, respectively, less than that for SPR. This indicates that the humidification rate is directly proportional to the surface area of the humidifier material. Consequently, during dehumidification, the maximum Y achieved with the use of the SPR-packed humidifier was approximately 1398 mL/h because it exhibited the maximum humidification rate. Meanwhile, the maximum Y achieved with TPR, LPR, ISR, and SFR was observed to be 1385, 1372, 1367, and 1343 mL/h. An analogous trend was observed for $\Delta T_{a,dehumid}$ and $\Delta T_{w,dehumid}$ (Fig. 9(b)) with the maximum air temperature reduction and water temperature increase of approximately 11.3 and 22.19 °C, respectively, for the HDH process with the SPR humidifier. Thus, the SPR was observed to be the most effective humidifier material to produce freshwater through the HDH process powered by low-grade waste heat energy.

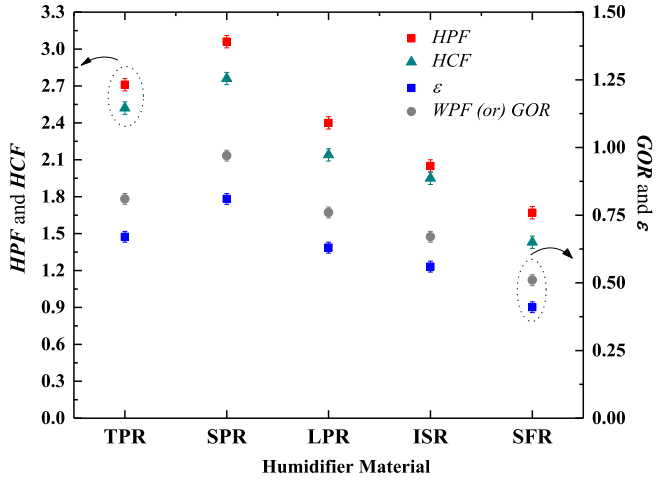

Fig. 10. Characteristics of various performance evaluation factors of humidifiers (for $\dot{m}_w$= 0.9 L/min, $\dot{m}_a$= 3.5 kg/min, $T_{a,humid\ in}$ = 70 °C, and $T_{w,humid\ in}$ = 55 °C).

7.6. Characteristics of various humidifier performance evaluation factors

For the optimum conditions across the humidifier and dehumidifier units, the various performance evaluation factors of humidifier packing material were compared as shown in Fig. 10. The maximum *GOR*, *HPF*, ε, and *HCF* of 0.97, 3.06, 0.81, and 2.76, respectively, were obtained for the HDH process with the adoption of the SPR humidifier packing material. Similarly, the minimum *GOR*, *HPF*, ε, and *HCF* of approximately 0.51, 1.67, 0.41, and 1.43, respectively, were achieved with the usage of the SFR humidifier material. The higher performance in the case of SPR could be attributed to the improved $\Delta T_{a,humid}$, $\Delta RH_{a,humid}$, $\Delta\omega_{a,humid}$, and $\Delta\dot{H}_{air,max}$ achieved with its usage during the humidification process as observed in the previous sections. The variation in the above properties has a synergic effect on the humidification and dehumidification performance of the HDH system. Thus, the various humidifier performance evaluation factors for different humidifier materials (Fig. 10) display a trend similar to that of the above properties (Fig. 9(a)). This is because these factors depend predominantly on the properties achieved across the HDH system. Thus, comparatively improved waste heat recovery potential and humidification effectiveness were achieved with the adoption of the SPR humidifier material. The variation in the humidifier performance factors with different humidifier materials considered in the present work (for the optimized conditions) as well as other key parameters are summarized and compared in Table 4.

7.7. Comparison with previous literature

Performance comparison of the present HDH system with the pre-existing systems is carried out in Table 5. It is noteworthy that an individual system's performance cannot be accounted only in terms of *Y*, as all the systems function with diverse operating conditions and heat energy input. Therefore, *GOR* is used as a baseline that represents the heat recovery potential of the individual systems. The *GOR* of the present system was identified to be higher than the systems that employed solar collectors for preheating [46–50], indicating the effectiveness of low-grade waste heat energy for preheating the fluids in HDH desalination systems. The higher *GOR* of the present system compared to Ref. [33] can be attributed to the dual-fluid preheating process in the case of the former that resulted in higher heat capacity compared to the latter. However, the *GOR* of the present system was lower than the HDH system in Ref. [30] that adopts the process of feed preheating using both heat pump waste heat and an additional solar collector. Therefore in addition to the higher heat energy input that contributes to better performance, its higher yield can be attributed to the lower coolant inlet temperature across the dehumidifier unit (18.39 °C) that can contribute to additional energy requirement for precooling. Nevertheless, the present system's performance can be further enhanced with optimized design modifications of the dehumidifier unit and thermally localized dehumidification process [51].

Table 5
Assessment of performance with previous systems.

System details	Corresponding *GOR*	Reference details
HDH system with feed preheated using evacuated tube solar collector	0.53	[47]
HDH system with feed preheated using solar water collector and thermal energy storage tank	0.63	[48]
HDH system with feed preheated using evacuated tube solar collector and heat pipe	0.65	[49]
HDH system with both air and feed preheated using dual-purpose solar collector	0.68	[50]
HDH system with both air and feed preheated using solar bubble column unit	0.78	[46]
HDH system with direct utilization of waste heat air from domestic air conditioning system	0.81	[33]
HDH system with both air and feed preheated using low-grade waste heat	0.97	[Present study]
HDH system with feed preheated using heat pump waste heat and solar collector	1.24	[30]

7.8. Physical and chemical water quality analysis

As the present study involved the direct utilization of seawater, its potable quality was evaluated in detail by physical and chemical analysis. The water quality tests were performed at Korea Research Institute of Ships & Ocean Engineering and Korea Polymer Testing & Research Institute. The various results obtained from the above analysis are summarized in Table 6. Detailed evaluation was carried out both for seawater (before the HDH process) and freshwater (after the HDH process). Furthermore, its quality was compared with the WHO and EPA drinking water standards. The physical water quality analysis revealed a significant reduction in the pH, TDS, and EC. The pH of seawater reduced from 8 to 6 (a reduction rate of 25%). Similarly, TDS and EC reduced significantly (from 9030 to 7.05 mg/L and 18,120 to 14.15 μs/cm, respectively). This indicated the potential of the low-grade waste heat-powered HDH desalination system for reducing the concentrations of salt and dissolved solids in seawater. Furthermore, an analysis of the primary ions including Na^+, Ca^{2+}, Mg^{2+}, and K^+ indicated that their

Table 4
Comparison of various performance evaluation factors of humidifiers (for optimum $\dot{m}_w$= 0.9 L/min, $\dot{m}_a$= 3.5 kg/min, $T_{a,humid\ in}$ = 70 °C, $T_{w,humid\ in}$ = 55 °C).

Humidifier material	$RH_{humidified\ air}$ (%)	$\Delta\omega_{air,humidifier}$ (g/kg)	*Y* (mL/h)	*HPF*	*HCF*	ε	*WPF/ GOR*
TPR	94.1	14.20	1385	2.71	2.52	0.67	0.81
SPR	97.7	16.23	1398	3.06	2.76	0.81	0.97
LPR	92.3	11.23	1372	2.40	2.14	0.63	0.76
ISR	89.5	10.54	1367	2.05	1.95	0.56	0.67
SFR	76.4	9.42	1343	1.67	1.43	0.41	0.51

Table 6
Comparative water quality analysis of seawater and freshwater.

Parameter (unit)	Seawater (before HDH)	Freshwater (after HDH)	WHO drinking water standards [52]	EPA drinking water standards [53]
pH	8	6	< 8.0	≤ 9.5
TDS (mg/L)	9030	7.05	1000	500
EC (μs/cm)	18,120	14.15	–	–
Sodium (mg/L)	10,728.05	0.125	50	30–60
Magnesium (mg/L)	5552.50	0.006	–	–
Calcium (mg/L)	5993.15	ND#	40	–
Potassium (mg/L)	4114.00	0.046	–	–
Strontium (mg/L)	7.28	0.899	–	–
Boron (mg/L)	4.96	0.0032	2.4	3
Arsenic (mg/L)	0.032	0.00006	0.01	0.01
Selenium (mg/L)	0.078	0.00432	0.04	0.05
Chromium (mg/L)	0.001881	0.000026	0.05	0.1
Cadmium (mg/L)	0.000033	0.000019	0.003	0.005
Mercury (mg/L)	0.000012	0.000009	0.006	0.002
Lead (mg/L)	0.000139	0.000008	0.01	–
Fluoride (mg/L)	< 0.1	< 0.1	1.5	0.8
Chloride (mg/L)	25,524	0.8	250	250
Nitrite (mg/L)	ND#	ND#	3	1
Bromide (mg/L)	ND#	ND#	–	10
Nitrate (mg/L)	ND#	ND#	50	50
Phosphate (mg/L)	ND#	ND#	–	–
Sulfate (mg/L)	2669	0.2	250	250

ND#- Non-detectable.

concentration reduced considerably to within the range of drinking water standards. This signified the efficacy of the developed system. Similarly, the concentrations of the major anions such as Cl^-, NO_2^-, NO_3^-, PO_4^{3-}, and SO_4^{2-} reduced to within acceptable limits for drinking water. Thus, Table 6 reveals that the developed low-grade waste heat-powered HDH system was capable of considerably reducing the concentrations of the ions and salts present in seawater to convert it into potable water when operated under optimized conditions. All the parameter values were well within the acceptable limits of potable water standards.

8. Conclusions

Experimental investigation and optimization of an HDH desalination system were carried out for its effective utilization with low-grade waste heat energy using varied surface area humidifier packing in conjunction with a detailed water quality analysis. The following are the observations based on the present work:

- Superior humidification and dehumidification performance are achieved under the optimum conditions of $\dot{m}_w$, $\dot{m}_a$, $T_{a,humid\ in}$, and $T_{w,humid\ in}$ (0.9 L/min, 3.5 kg/min, 70 °C, and 55 °C, respectively) across the humidifier and dehumidifier units. It is determined that the humidification rate depends primarily on the air fluid properties. Moreover, the dehumidification rate depends on the feed water properties in a closed air–open water HDH cycle.
- The maximum *Y* and HDH performance efficiency are achieved for higher $T_{a,humid\ in}$, $\dot{m}_a$, and $T_{w,humid\ in}$ by directly utilizing seawater as a coolant across the dehumidifier without any precooling mechanism.
- The wet surface area of the humidifier packing material chiefly influences the humidification efficiency and thereby, the freshwater productivity during the dehumidification process. Thus, comparatively improved $RH_{a,humid\ out}$, $\Delta\omega_{a,humid}$, *Y*, *HPF*, *HCF*, ε, and *WPF* of 97.7%, 16.23 g/kg, 1398 mL/h, 3.06, 2.76, 0.81, and 0.97, respectively, are achieved by using SPR humidifier packing with enhanced surface area.
- The mechanism of interconnected feed water flow from the dehumidifier to the humidifier unit aided in the preheating of the feed during its passage. However, it was determined that the individual feed water flow across the humidifier and dehumidifier units can contribute to a higher *Y*.
- A significant reduction in concentrations of salt, dissolved solids, and ions were revealed by the water quality analysis indicating the efficacy of the HDH technique for producing potable water using low-grade waste heat energy.

Further design modifications of the dehumidifier unit can contribute to an improved dehumidification process and thereby, a higher *Y* from the HDH system.

Nomenclature

AC	Air conditioner
i	Corresponding TPR (or) SPR (or) LPR (or) ISR (or) SFR humidifier packing
EC	Electrical conductivity (μs/cm)
U_{GOR}	Experimental uncertainty of gained output ratio
U_ε	Experimental uncertainty of humidification effectiveness factor
U_{HPF}	Experimental uncertainty of humidification performance potential factor
FTHE	Finned tube heat exchanger
GOR	Gained output ratio
HMT	Heat and mass transfer
HCF	Heat capacity ratio factor of humidifier
HVAC	Heat, ventilation, and air conditioning
HDH	Humidification–dehumidification
HPF	Humidification performance potential factor
LPR	Large pall ring
PV	Photovoltaic
PVT	Photovoltaic thermal
PVC	Polyvinyl chloride
RH	Relative humidity (%)
SPR	Small pall ring
SFR	Snowflake ring
ISR	Super intalox saddle ring
TDS	Total dissolved solids (mg/L)
TPR	Tri-pack ring
EPA	United States Environmental Protection Agency
WPF	Waste-heat recovery potential factor
WHO	World Health Organization
$h_{a,preheat\ in}$	Air enthalpy across preheater entry (kJ/kg)
$h_{a,preheat\ out}$	Air enthalpy across preheater exit (kJ/kg)
$RH_{a,humid\ out}$	Air relative humidity across humidifier exit (°C)
$T_{a,humid\ in}$	Air temperature across humidifier entry (°C)
$T_{a,humid\ out}$	Air temperature across humidifier exit (°C)
$\Delta\dot{H}_{air,max}$	Enthalpy rate difference of air (kJ/kg)
$\Delta\dot{H}_{feed,max}$	Enthalpy rate difference of feed (kJ/kg)
$T_{w,humid\ in}$	Feed temperature across humidifier entry (°C)

$T_{w,humid\ out}$ Feed temperature across humidifier exit (°C)
$T_{w,preheat\ in}$ Feed water temperature across preheater entry (°C)
$T_{w,preheat\ out}$ Feed water temperature across preheater exit (°C)
ε Humidification effectiveness of humidifier
$\Delta\omega_{a,humid}$ Humidity ratio increment across humidifier (g/kg)
$\omega_{a,humid\ in}$ Humidity ratio of air across humidifier entry (g/kg)
$\omega_{a,humid\ out}$ Humidity ratio of air across humidifier exit (g/kg)
$\omega_{a,humid\ out,s}$ Humidity ratio when the humidified air is saturated (g/kg)
γ Latent heat of condensation (kJ/kg)
L Latent heat of water (kJ/kg)
$\dot{m}_a$ Mass flow rate of air (kg/s)
$\dot{m}_w$ Mass flow rate of feed water (L/min)
$\Delta RH_{a,humid}$ Relative humidity increment of air across humidifier (%)
C_{pa} Specific heat of the air (kJ/kgK)
C_{pw} Specific heat of the feed (kJ/kgK)
$\Delta T_{w,dehumid}$ Temperature increment of feed across dehumidifier (°C)
T_a Temperature of air (°C)
T_w Temperature of feed water (°C)
$\Delta T_{a,dehumid}$ Temperature reduction of air across dehumidifier (°C)
$\Delta T_{a,humid}$ Temperature reduction of air across humidifier (°C)
Q_{in} Thermal energy input to the humidifier unit (kJ/h)
Y Yield (mL/h)

Declaration of Competing Interest

The authors declare that they have no known competing financial interests or personal relationships that could have appeared to influence the work reported in this paper.

Acknowledgement

The authors gratefully acknowledge the financial support provided for this work by the ERICA ERICA Industry-University Cooperation Foundation, Hanyang University, Republic of Korea (HY-2021). The authors would also like to thank the Research Scholars of the Energy & Environmental Engineering Laboratory, Department of Mechanical Engineering, Hanyang University for their efforts during the fabrication of the experimental set-up.

References

[1] I. Ihsanullah, M.A. Atieh, M. Sajid, M.K. Nazal, Desalination and environment: a critical analysis of impacts, mitigation strategies, and greener desalination technologies, Sci. Total Environ. 780 (2021), 146585, https://doi.org/10.1016/j.scitotenv.2021.146585.
[2] Ihsanullah, Carbon nanotube membranes for water purification: developments, challenges, and prospects for the future, Sep. Purif. Technol. 209 (2019) 307–337, https://doi.org/10.1016/j.seppur.2018.07.043.
[3] M.A. Jamil, M.W. Shahzad, S.M. Zubair, A comprehensive framework for thermoeconomic analysis of desalination systems, Energy Convers. Manag. 222 (2020), 113188, https://doi.org/10.1016/j.enconman.2020.113188.
[4] H. Sharon, K.S. Reddy, A review of solar energy driven desalination technologies, Renew. Sustain. Energy Rev. 41 (2015) 1080–1118, https://doi.org/10.1016/j.rser.2014.09.002.
[5] E. Jones, M. Qadir, M.T.H. van Vliet, V. Smakhtin, Kang S. Mu, The state of desalination and brine production: a global outlook, Sci. Total Environ. 657 (2019) 1343–1356, https://doi.org/10.1016/j.scitotenv.2018.12.076.
[6] A. Al-Karaghouli, L.L. Kazmerski, Energy consumption and water production cost of conventional and renewable-energy-powered desalination processes, Renew. Sustain. Energy Rev. 24 (2013) 343–356, https://doi.org/10.1016/j.rser.2012.12.064.
[7] S.A. Kalogirou, Seawater desalination using renewable energy sources, Prog. Energy Combust. Sci. 31 (2005) 242–281, https://doi.org/10.1016/j.pecs.2005.03.001.
[8] A. Kasaeian, S. Babaei, M. Jahanpanah, H. Sarrafha, A. Sulaiman Alsagri, S. Ghaffarian, et al., Solar humidification-dehumidification desalination systems: a critical review, Energy Convers. Manag. 201 (2019), https://doi.org/10.1016/j.enconman.2019.112129.
[9] F. Alnaimat, M. Ziauddin, B. Mathew, A review of recent advances in humidification and dehumidification desalination technologies using solar energy, Desalination 499 (2021), 114860, https://doi.org/10.1016/j.desal.2020.114860.
[10] S.A. El-Agouz, R. Sathyamurthy, Manokar A. Muthu, Improvement of humidification–dehumidification desalination unit using a desiccant wheel, Chem. Eng. Res. Des. 131 (2018) 104–116, https://doi.org/10.1016/j.cherd.2017.06.004.
[11] E. Deniz, S. Çınar, Energy, exergy, economic and environmental (4E) analysis of a solar desalination system with humidification-dehumidification, Energy Convers. Manag. 126 (2016) 12–19, https://doi.org/10.1016/j.enconman.2016.07.064.
[12] G.P. Narayan, M.H. Sharqawy, E.K. Summers, J.H. Lienhard, S.M. Zubair, M. A. Antar, The potential of solar-driven humidification-dehumidification desalination for small-scale decentralized water production, Renew. Sustain. Energy Rev. 14 (2010) 1187–1201, https://doi.org/10.1016/j.rser.2009.11.014.
[13] D.U. Lawal, N.A.A. Qasem, Humidification-dehumidification desalination systems driven by thermal-based renewable and low-grade energy sources: a critical review, Renew. Sustain. Energy Rev. 125 (2020), 109817, https://doi.org/10.1016/j.rser.2020.109817.
[14] R. Santosh, T. Arunkumar, R. Velraj, G. Kumaresan, Technological advancements in solar energy driven humidification-dehumidification desalination systems - a review, J. Clean. Prod. 207 (2019) 826–845, https://doi.org/10.1016/j.jclepro.2018.09.247.
[15] S.M. Shalaby, A.E. Kabeel, B.M. Moharram, A.H. Fleafl, Experimental study of hybrid solar humidification dehumidification system for extremely saline water desalination, Energy Convers. Manag. 235 (2021), 114021, https://doi.org/10.1016/j.enconman.2021.114021.
[16] W. He, H. Yang, T. Wen, D. Han, Thermodynamic and economic investigation of a humidification dehumidification desalination system driven by low grade waste heat, Energy Convers. Manag. 183 (2019) 848–858, https://doi.org/10.1016/j.enconman.2018.10.044.
[17] W.F. He, D. Han, W.P. Zhu, C. Ji, Thermo-economic analysis of a water-heated humidification-dehumidification desalination system with waste heat recovery, Energy Convers. Manag. 160 (2018) 182–190, https://doi.org/10.1016/j.enconman.2018.01.048.
[18] W.F. He, L.N. Xu, D. Han, L. Gao, Performance analysis of an air-heated humidification-dehumidification desalination plant powered by low grade waste heat, Energy Convers. Manag. 118 (2016) 12–20, https://doi.org/10.1016/j.enconman.2016.03.073.
[19] K. Srithar, T. Rajaseenivasan, M. Arulmani, R. Gnanavel, M. Vivar, M. Fuentes, Energy recovery from a vapour compression refrigeration system using humidification dehumidification desalination, Desalination 439 (2018) 155–161, https://doi.org/10.1016/j.desal.2018.04.008.
[20] H. Sayyaadi, G. Ghorbani, Conceptual design and optimization of a small-scale dual power-desalination system based on the Stirling prime-mover, Appl. Energy 223 (2018) 457–471, https://doi.org/10.1016/j.apenergy.2018.04.077.
[21] W.F. He, F. Wu, Y.P. Kong, T. Wen, J.J. Chen, D. Han, Parametric analysis of a power-water cogeneration system based on single-extraction organic Rankine cycle, Appl. Therm. Eng. 148 (2019) 382–390, https://doi.org/10.1016/j.applthermaleng.2018.11.070.
[22] W. He, H. Yang, D. Han, Thermodynamic investigation and optimization of a heat pump coupled open-air, open-water humidification dehumidification desalination system with a direct contact dehumidifier, Desalination 469 (2019), 114101, https://doi.org/10.1016/j.desal.2019.114101.
[23] P. Gabrielli, M. Gazzani, N. Novati, L. Sutter, R. Simonetti, L. Molinaroli, et al., Combined water desalination and electricity generation through a humidification-dehumidification process integrated with photovoltaic-thermal modules: design, performance analysis and techno-economic assessment, Energy Convers. Manag. X 1 (2019), 100004, https://doi.org/10.1016/j.ecmx.2019.100004.
[24] W.F. He, D. Han, C. Ji, Investigation on humidification dehumidification desalination system coupled with heat pump, Desalination 436 (2018) 152–160, https://doi.org/10.1016/j.desal.2018.02.021.
[25] W.F. He, J.J. Chen, M.R. Zhen, D. Han, Thermodynamic, economic analysis and optimization of a heat pump driven desalination system with open-air humidification dehumidification configurations, Energy 174 (2019) 768–778, https://doi.org/10.1016/j.energy.2019.03.005.
[26] W.F. He, T. Wen, D. Han, L.T. Luo, R.Y. Li, W.C. Zhong, Energetic, entropic and economic analysis of a heat pump coupled humidification dehumidification desalination system using a packed bed dehumidifier, Energy Convers. Manag. 194 (2019) 11–21, https://doi.org/10.1016/j.enconman.2019.04.038.
[27] N.A.A. Qasem, S.M. Zubair, Performance evaluation of a novel hybrid humidification-dehumidification (air-heated) system with an adsorption desalination system, Desalination 461 (2019) 37–54, https://doi.org/10.1016/j.desal.2019.03.011.
[28] A. Giwa, H. Fath, S.W. Hasan, Humidification-dehumidification desalination process driven by photovoltaic thermal energy recovery (PV-HDH) for small-scale sustainable water and power production, Desalination 377 (2016) 163–171, https://doi.org/10.1016/j.desal.2015.09.018.
[29] A.M. Elsafi, Integration of humidification-dehumidification desalination and concentrated photovoltaic-thermal collectors: energy and exergy-costing analysis, Desalination 424 (2017) 17–26, https://doi.org/10.1016/j.desal.2017.09.022.
[30] H. Xu, Y. Zhao, T. Jia, Y.J. Dai, Experimental investigation on a solar assisted heat pump desalination system with humidification-dehumidification, Desalination 437 (2018) 89–99, https://doi.org/10.1016/j.desal.2018.03.001.
[31] H. Xu, Y. Zhao, Y.J. Dai, Experimental study on a solar assisted heat pump desalination unit with internal heat recovery based on humidification-dehumidification process, Desalination 452 (2019) 247–257, https://doi.org/10.1016/j.desal.2018.11.019.
[32] M.B. Shafii, H. Jafargholi, M. Faegh, Experimental investigation of heat recovery in a humidification-dehumidification desalination system via a heat pump, Desalination 437 (2018) 81–88, https://doi.org/10.1016/j.desal.2018.03.004.

[33] R. Santosh, G. Kumaresan, S. Selvaraj, T. Arunkumar, R. Velraj, Investigation of humidification-dehumidification desalination system through waste heat recovery from household air conditioning unit, Desalination 467 (2019) 1–11, https://doi.org/10.1016/j.desal.2019.05.016.
[34] R. Santosh, G. Kumaresan, G.K. Kumar, R. Velraj, Experimental parametric investigation of waste heat powered humidification dehumidification system for production of freshwater from wastewater, Desalination 484 (2020), 114422, https://doi.org/10.1016/j.desal.2020.114422.
[35] J.H. Wang, N.Y. Gao, Y. Deng, Y.L. Li, Solar power-driven humidification-dehumidification (HDH) process for desalination of brackish water, Desalination 305 (2012) 17–23, https://doi.org/10.1016/j.desal.2012.08.008.
[36] M.S. Elzayed, M.A.M. Ahmed, N.A.A. Qasem, M.A. Antar, S.M. Zubair, A design procedure to size thermodynamically-balanced humidification-dehumidification desalination systems, Energy Convers. Manag. 224 (2020), 113357, https://doi.org/10.1016/j.enconman.2020.113357.
[37] R. Santosh, G. Kumaresan, S. Monisha, G.K. Kumar, R. Velraj, Experimental evaluation of PVA as novel humidifier material for humidification-dehumidification applications, J. Test. Eval. 49 (2021) 20190722, https://doi.org/10.1520/jte20190722.
[38] K. Thanaiah, V. Gumtapure, Tadesse G. Mitiku, Experimental analysis on humidification-dehumidification desalination system using different packing materials with baffle plates, Therm. Sci. Eng. Prog. 22 (2021), 100831, https://doi.org/10.1016/j.tsep.2020.100831.
[39] IEA, Thinking about energy and water together can help ensure that “no one is left behind”, International Energy Agency (IEA), Paris, 2019. https://www.iea.org/commentaries/thinking-about-energy-and-water-together-can-help-ensure-that-no-one-is-left-behind.
[40] J. Maćkowiak, Progress in design of random packing for gas-liquid systems, Chem. Eng. Res. Des. 99 (2015) 28–42, https://doi.org/10.1016/j.cherd.2015.05.038.
[41] G.P. Narayan, M.G. St. John, S.M. Zubair, J.H. Lienhard, Thermal design of the humidification dehumidification desalination system: an experimental investigation, Int. J. Heat Mass Transf. 58 (2013) 740–748, https://doi.org/10.1016/j.ijheatmasstransfer.2012.11.035.
[42] K. Park, J.S. Mok, A.R. Ryu, J.Y. Kwon, I.T. Ham, K.B. Shim, Occurrence and virulence of Vibrio parahaemolyticus isolated from seawater and bivalve shellfish of the Gyeongnam coast, Korea, in 2004–2016, Mar. Pollut. Bull. 137 (2018) 382–387, https://doi.org/10.1016/j.marpolbul.2018.10.033.
[43] H.A. Ahmed, I.M. Ismail, W.F. Saleh, M. Ahmed, Experimental investigation of humidification-dehumidification desalination system with corrugated packing in the humidifier, Desalination 410 (2017) 19–29, https://doi.org/10.1016/j.desal.2017.01.036.
[44] N.C. Barford, Experimental Measurements: Precision, Error and Truth, 2nd ed., John Wiley & Sons, New York, 1990.
[45] S.J. Kline, F.A. McClintock, Describing uncertainties in single sample experiments, Mech. Eng. 75 (1953) 3–8.
[46] K. Srithar, T. Rajaseenivasan, Performance analysis on a solar bubble column humidification dehumidification desalination system, Process Saf. Environ. Prot. 105 (2017) 41–50, https://doi.org/10.1016/j.psep.2016.10.002.
[47] A. Khalil, S.A. El-Agouz, Y.A. El-Samadony, A. Abdo, Solar water desalination using an air bubble column humidifier, Desalination 372 (2015) 7–16, https://doi.org/10.1016/j.desal.2015.06.010.
[48] S.A. El-Agouz, G.B. Abd El-Aziz, A.M. Awad, Solar desalination system using spray evaporation, Energy 76 (2014) 276–283, https://doi.org/10.1016/j.energy.2014.08.009.
[49] P. Behnam, M.B. Shafii, Examination of a solar desalination system equipped with an air bubble column humidifier, evacuated tube collectors and thermosyphon heat pipes, Desalination 397 (2016) 30–37, https://doi.org/10.1016/j.desal.2016.06.016.
[50] T. Rajaseenivasan, K. Srithar, Potential of a dual purpose solar collector on humidification dehumidification desalination system, Desalination 404 (2017) 35–40, https://doi.org/10.1016/j.desal.2016.10.015.
[51] Z. Xu, L. Zhang, L. Zhao, B. Li, B. Bhatia, C. Wang, K.L. Wilke, Y. Song, O. Labban, J.H. Lienhard, R. Wang, Ultrahigh-efficiency desalination via a thermally-localized multistage solar still, Energy Environ. Sci. 13 (3) (2020) 830–839, https://doi.org/10.1039/c9ee04122b.
[52] The World Health Organization, Guidelines for Drinking-water Quality. https://www.who.int/publications/i/item/9789241549950, 2017.
[53] United States Environmental Protection Agency, 2018 Edition of the Drinking Water Standards and Health Advisories Tables. https://www.epa.gov/sites/default/files/2018-03/documents/dwtable2018.pdf, 2018.